Chinese Physics B

RAPID COMMUNICATION

Slight Co-doping tuned magnetic and electric properties on cubic $BaFeO_3$ single crystal

To cite this article: Shijun Qin *et al* 2022 *Chinese Phys. B* **31** 097503

RAPID COMMUNICATION

Slight Co-doping tuned magnetic and electric properties on cubic $BaFeO_3$ single crystal

Shijun Qin(覃浞俊)[1,2], Bowen Zhou(周博文)[1,2], Zhehong Liu(刘哲宏)[1,2], Xubin Ye(叶旭斌)[1,2], Xueqiang Zhang(张雪强)[1], Zhao Pan(潘昭)[1,2], and Youwen Long(龙有文)[1,2,3,†]

[1] *Beijing National Laboratory for Condensed Matter Physics, Institute of Physics, Chinese Academy of Sciences, Beijing* 100190, *China*
[2] *School of Physical Sciences, University of Chinese Academy of Sciences, Beijing* 100049, *China*
[3] *Songshan Lake Materials Laboratory, Dongguan* 523808, *China*

(Received 5 May 2022; revised manuscript received 27 May 2022; accepted manuscript online 2 June 2022)

The single crystal of cubic perovskite $BaFeO_3$ shows multiple magnetic transitions and external stimulus sensitive magnetism. In this paper, a 5%-Co-doped $BaFeO_3$ (*i.e.* $BaFe_{0.95}Co_{0.05}O_3$) single crystal was grown by combining floating zone methods with high-pressure techniques. Such a slight Co doping has little effect on crystal structure, but significantly changes the magnetism from the parent antiferromagnetic ground state to a ferromagnetic one with the Curie temperature $T_C \approx 120$ K. Compared with the parent $BaFeO_3$ at the induced ferromagnetic state, the saturated magnetic moment of the doped $BaFe_{0.95}Co_{0.05}O_3$ increases by about 10% and reaches 3.64 μ_B/f.u. Resistivity and specific heat measurements show that the ferromagnetic ordering favors metallic-like electrical transport behavior for $BaFe_{0.95}Co_{0.05}O_3$. The present work indicates that Co-doping is an effective method to tune the magnetic and electric properties for the cubic perovskite phase of $BaFeO_3$.

Keywords: floating-zone single crystal, high-pressure synthesis, chemical doping, magnetic and electrical properties

PACS: 75.30.Et, 75.10.Lp, 81.10.Fq, 81.40.Vw **DOI:** 10.1088/1674-1056/ac7549

1. Introduction

Perovskite oxides $AFeO_3$ (A = Ca, Sr, and Ba) with unusually high Fe^{4+} state show very interesting structural and physical properties.[1–7] At room temperature, $CaFeO_3$ crystallizes to an orthorhombic *Pnma* structure. As the temperature decreases to about 290 K, a so-called charge disproportionation ($2Fe^{4+} \rightarrow Fe^{3+} + Fe^{5+}$) takes place, leading to a metal-insulator transition as well as a *Pnma* to $P2_1/n$ structural phase transition. On further cooling to 116 K, a helical antiferromagnetic (AFM) phase transition is observed, with the spin propagation vector along the pseudocubic [111] direction.[2,3] In comparison with $CaFeO_3$, the crystal structure of $SrFeO_3$ changes to a simple cubic perovskite with space Pm-3m, which exhibits a helical AFM ordering at $T_{N1} \approx$ 134 K. On further cooling, $SrFeO_3$ undergoes another two AFM transitions respectively at $T_{N2} \approx 110$ K and $T_{N3} \approx 56$ K due to the higher-order spiral order adjustment.[4,7–10] Therefore, the helical AFM transitions of $SrFeO_3$ seem rather complex, and even topological magnetic structures which have two kinds of multiple-$\boldsymbol{q}$ spin structures has been proposed recently.[11] In spite of complicated spin transitions, $SrFeO_3$ always shows metallic electrical transport behavior.[4] Compared with the easily synthesized cubic perovskite phase of $SrFeO_3$, such a simple cubic phase is very difficult to prepare for the analogue $BaFeO_3$. Since the ionic radius of Ba^{2+} is considerably larger than that of Sr^{2+},[12] conventional annealing always leads to the presence of a hexagonal phase for $BaFeO_3$.[13] Until 2011, the simple cubic perovskite phase $BaFeO_3$ was obtained by a topological chemical oxidization method for the precursor $BaFeO_{2.5}$ at lower temperature (473 K) using ozone as an oxidizing agent. However, such a surface oxidization method can only obtain a small amount of powder samples with the thickness about 1 μm.[14] Most recently, large-size single crystals (> 3 mm) for the cubic perovskite phase of $BaFeO_3$ are successful for growth by using floating zone methods combined with high-pressure treatment techniques.[15] The $BaFeO_3$ single crystal also shows three magnetic phase transitions. With decreasing temperature, a spin glass transition is found to occur at $T_{SG} \approx 181$ K, followed by two long-range helical AFM transitions at about 117 K and 97 K, respectively. Moreover, a semiconductor-metal-like transition occurs near 117 K.[15] These complicated magnetic behaviors indicate competing ferromagnetic (FM) and AFM interactions in $BaFeO_3$.

Because of the helical magnetic structure, the magnetism of $AFeO_3$ are highly sensitive to external stimuli such as pressure and chemical doping. For example, $CaFeO_3$ experiences a structural phase transition and a spin state transition at a critical around 30 GPa.[16] The AFM ground state of $SrFeO_3$ can be tuned into an FM one if one uses a pressure up to

†Corresponding author. E-mail: ywlong@iphy.ac.cn

7 GPa[17] or doping with Co for Fe by 20%.[18] Compared with $SrFeO_3$, the AFM and FM competition is more remarkable in $BaFeO_3$.[19] Therefore, it is very interesting to study the chemical doping effects on the magnetic and electrical properties of the cubic $BaFeO_3$. In this paper, we found that a tiny Co doping for Fe by 5% in nominal can change the AFM ground state of $BaFeO_3$ to an FM state in $BaFe_{0.95}Co_{0.05}O_3$ single crystal. Different electrical transport properties are also observed by such a small chemical doping.

2. Experimental details

The polycrystalline $BaFe_{0.95}Co_{0.05}O_{2.5}$ precursors were prepared by a solid-state reaction method.[15,20] Appropriate amounts of highly pure (99.9%) $BaCO_3$, Fe_2O_3, and Co_3O_4 were stoichiometrically weighed, and fully mixed and ground. The mixed powders were heated at 1373 K for 24 hours under flowing Ar gas. The resulting product was reground in air and pressed into a rod of 4.0 mm in diameter and 8.0 mm in length at 200 MPa for annealing at 1373 K for 12 hours in flowing Ar. The annealing rod was adopted to grow the oxygen deficient $BaFe_{0.95}Co_{0.05}O_{2.5}$ single crystals by using the floating zone method with a growth rate of 2.4 mm/h at Ar atmosphere. To obtain oxygen stoichiometric $BaFe_{0.95}Co_{0.05}O_3$ single crystal, the oxygen deficient precursor of $BaFe_{0.95}Co_{0.05}O_{2.5}$ single crystal was treated on a large volume cubic-anvil-type high-pressure apparatus at 5 GPa and 1023 K for 60 min with the usage of exceeding $KClO_4$ oxidizing agent.[15,18,20]

Powder x-ray diffraction (XRD) and Laue back reflection were used to identify the crystal quality and structure on a Huber diffractometer at room temperature with Cu $K\alpha_1$ radiation. The diffraction range of 2θ angle is from 10° to 100° with a step of 0.005°. Structural refinement for the XRD data was performed based on the Rietveld method using the GSAS program.[21] An Setaram TG-DTA system was used to perform thermogravimetric (TG) analysis with a heating rate of 10 K/min to 1300 K in Ar flow. The temperature-dependent magnetic susceptibility and isothermal magnetization were measured using a superconducting quantum interference device magnetometer (Quantum Design, MPMS3-VSM). Specific heat and resistivity data were obtained on a physical property measurement system (Quantum Design, PPMS-9T) at zero magnetic field.

3. Results and discussion

Figure 1(a) shows the precursor single crystal of $BaFe_{0.95}Co_{0.05}O_{2.5}$ and full oxidization $BaFe_{0.95}Co_{0.05}O_3$ single crystal with ~ 3 mm in diameter and height. In order to facilitate the anisotropy study of the physical properties of the single crystal, we used Laue diffraction to determine the crystal planes and cut specific planes for physical property measurements. The bulk XRD pattern was performed on the selected (100) plane of $BaFe_{0.95}Co_{0.05}O_3$ crystal with the size of 2 mm × 2 mm × 1 mm as shown in Fig. 1(b), only $h00$ peaks can be observed, suggesting that the as-made crystals are of single domain without observed twins. The insets of Fig. 1(b) show the sharp Laue diffraction spots of the high symmetrical (001), (110), and (111) planes, which further confirm the high quality of $BaFe_{0.95}Co_{0.05}O_3$ single crystal we obtained. Furthermore, this doped single crystal were crushed into powders for XRD measurement. The powder XRD pattern as well as the Rietveld refinement results are presented in Fig. 1(c). One can find that all the diffraction peaks can be well fitted based on a simple cubic perovskite structure with space group *Pm*-3*m*. The refined structural parameters are shown in Table 1. Compared with the parent single crystal of $BaFeO_3$ with $a = 3.96833$ Å,[15] the refined lattice constant of $BaFe_{0.95}Co_{0.05}O_3$ crystal slightly increases to 3.97131(7) Å. The lattice expansion results from the covalent effect of B–O in cubic $BaFeO_3$ weakened by Co doping, and the B–O bond length increased.

Table 1. Refined structure parameters for $BaFe_{0.95}Co_{0.05}O_3$ single crystal at room temperature[a].

Parameter	Value	Parameter	Value
a (Å)	3.97131(7)	Ba–O (Å) ×12	2.80814(3)
V (Å^3)	62.633(3)	Fe/Co–O (Å) ×6	1.98565(3)
Uiso(Ba) ($100 \times$ Å^2)	0.32(2)	R_{wp} (%)	2.8
Uiso(Fe/Co) ($100 \times$ Å^2)	0.54(4)	R_p (%)	1.9
Uiso(O) ($100 \times$ Å^2)	0.58(1)		

[a]Space group *Pm*-3*m* (No. 221); atomic sites are Ba 1*a* (0, 0, 0), Fe/Co 1*b* (0.5, 0.5, 0.5), and O 3*c* (0.5, 0.5, 0).

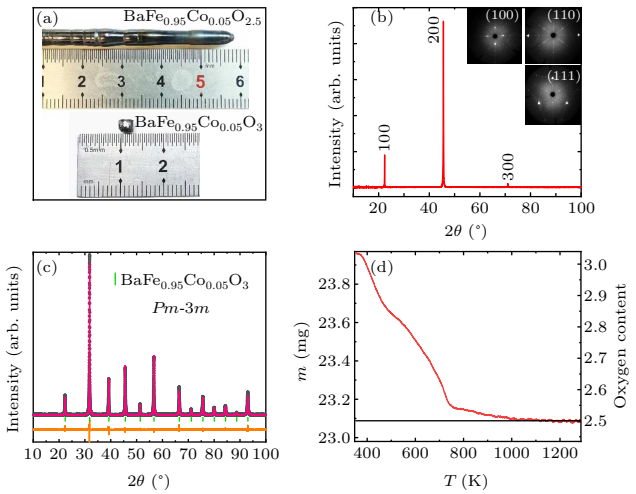

Fig. 1. (a) Morphology of $BaFe_{0.95}Co_{0.05}O_{2.5}$ and $BaFe_{0.95}Co_{0.05}O_3$ single crystals. (b) XRD pattern for the high symmetrical (001) plane of the $BaFe_{0.95}Co_{0.05}O_3$ single crystal. The inset shows the Laue diffraction spots of the (100), (110), and (111) planes. (c) Powder XRD pattern measured at room temperature and Rietveld refinement results of pulverized $BaFe_{0.95}Co_{0.05}O_3$ single crystal. The observed (black circles), calculated (pink line), and difference (orange line) patterns are shown. The green ticks indicate the allowed Bragg reflections with space group *Pm*-3*m*. (d) Temperature-dependent mass and oxygen content of $BaFe_{0.95}Co_{0.05}O_3$ single crystal.

Considering that the oxygen content has significant influence on physical properties of materials, the TG measurement was performed to examine the oxygen content of $BaFe_{0.95}Co_{0.05}O_3$ single crystal. Figure 1(d) shows the sample mass as a function of temperature. Obviously, the oxygen starts to release at about 370 K. At temperatures above 1000 K, the decomposed product becomes stable. According to the mass loss and the final product, which is the precursor $BaFe_{0.95}Co_{0.05}O_{2.5}$ as confirmed by XRD, the calculated oxygen content of $BaFe_{0.95}Co_{0.05}O_3$ single crystal is determined to be 3.01(2), indicating the stoichiometric composition for the single crystal we grown. This result in turn suggests the presence of Fe^{4+}/Co^{4+} valence states in $BaFe_{0.95}Co_{0.05}O_3$ as reported in $SrFeO_3$ [4] and $SrCoO_3$ [20] single crystals.

Figure 2(a) shows the temperature dependence of magnetic susceptibility (χ) of $BaFe_{0.95}Co_{0.05}O_3$ single crystal with an applying magnetic field ($H = 0.1$ T) parallel to the (100), (110), and (111) crystal planes in a field-cooling mode. As the temperature decreases to a critical temperature $T_C \approx 120$ K, the magnetic susceptibility experiences a sharp increase, indicting an FM phase transition. One can find that there is no significant difference in the susceptibility curves with field along different crystal planes, suggesting negligible magnetocrystalline anisotropy in the cubic perovskite phase of $BaFe_{0.95}Co_{0.05}O_3$. The inset of Fig. 2(a) shows the inverse susceptibility as function of temperature. Above 240 K, the data can be fitted based on the Curie–Weiss law with the function $\chi^{-1} = (T - \theta)/C$. The fitted Weiss temperature $\theta = 175.7$ K is in agreement with the FM ordering. According to the fitted Curie constant $C = 4.199$ emu·K·mol^{-1}, the effective magnetic moment is calculated to be 5.79 μ_B/f.u. If one considers the spin-only contribution for a high-spin Fe^{3+} (Fe^{4+}) state, the effective moment per ion in theory should be 5.89 (4.90) μ_B. Because of the strong p–d negative charge transfer energy, the high $Fe^{4+}(3d^4)$ state can be regard as an $Fe^{3+}(3d^5)$ combined with an oxygen hole $\underline{L}$, (*i.e.*, a $d^5\underline{L}$ state).[15,22] The Curie–Weiss fitting seems to suggest the formation of such a $d^5\underline{L}$ state in $BaFe_{0.95}Co_{0.05}O_3$.

Figure 2(b) depicts the isothermal magnetization curves measured at selected temperatures with the magnetic field parallel to the (100) plane. Above T_C, the linear magnetization behavior is consistent with the paramagnetism. Below T_C (*e.g.* at 100, 15, and 2 K), however, canonical magnetic hysteresis is found to occur. Moreover, the magnetization sharply increases with field and becomes saturated at 1.0 T. The coercive field is quite small (13.6 Oe at 2 K, 1 Oe = 79.5775 A·m^{-1}), indicating the soft FM feature. The saturated magnetic moment observed at 2 K and 6 T is 3.64 μ_B/f.u., which is somewhat larger than that of the parent $BaFeO_3$ single crystal (3.2 μ_B/f.u.).[15] Figure 2(c) shows the comparison of magnetization with field along the three typical planes of (100), (110), and (111). Basically, there is no essential difference occurring in these three directions. At this stage, it is difficult to distinguish the easiest magnetization axis from [110] and [111] directions. Sharply different from $BaFeO_3$ where the magnetization undergoes a clear metamagnetic transition at ~ 0.5 T from the initial AFM ground state to a higher-field FM state, the ground spin state of the Co-5% doped system has already been FM without any metamagnetic variation taking place.

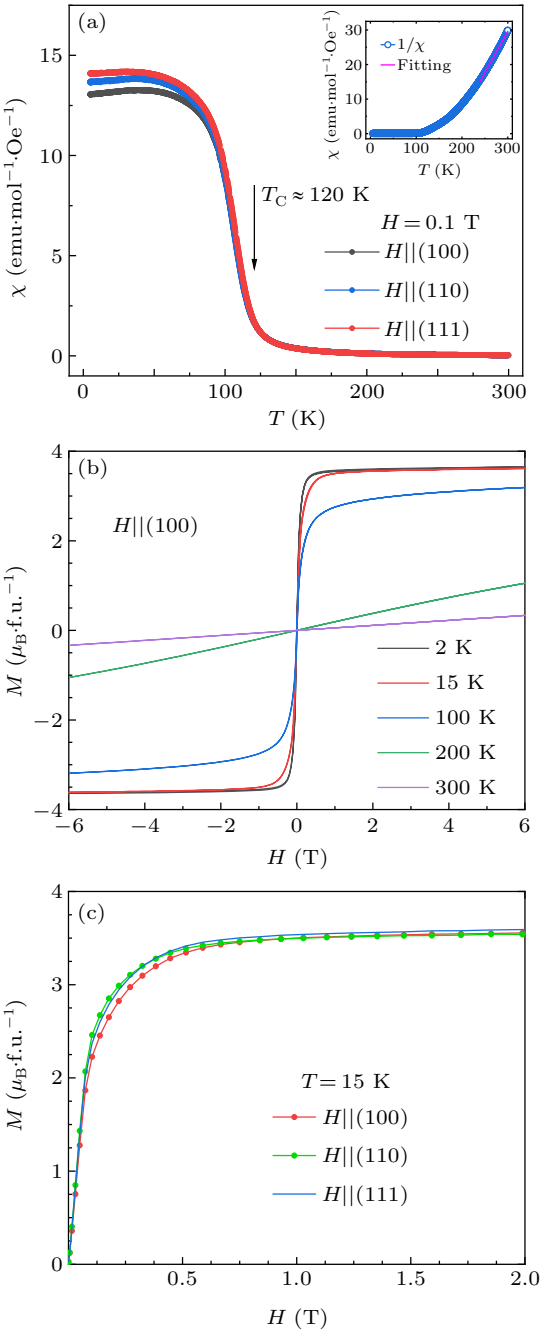

Fig. 2. (a) The temperature-dependent magnetic susceptibility of $BaFe_{0.95}Co_{0.05}O_3$ single crystal measured at 0.1 T with magnetic field parallel to the (100), (110), and (111) planes. The inset shows the Curie–Weiss fitting for the inverse susceptibility in 240 K–300 K. (b) Isothermal magnetization curves measured at selected temperatures with the field parallel to the (100) plane. (c) Comparison of field-dependent magnetization curves with field parallel to the (100), (110), and (111) planes.

In $SrFe_{1-x}Co_xO_3$ solid solution, the Co-doping induced FM phase does not appear until the substitution content of Co increase to 20%.[18] Therefore, the cubic $BaFeO_3$ is more sensitive to be tailored than $SrFeO_3$.The propagation vector expression of the spiral spin ordering of the cubic Sr/$BaFeO_3$ is $\boldsymbol{Q} = \varphi \times (2\pi/a)$,[11,14,23] where a is the lattice constant. The spin arrangement thus depends largely on the value of the spiral angle φ. For example, if $\varphi = 0$, the spins will all align in parallel and an FM state occurs. The value of φ for $BaFeO_3$ and $SrFeO_3$ is 0.06 and 0.112,[23] respectively. Therefore, a slight Co-doping only by 5% can induce the ground spin state transition from helical AFM to collinear FM for $BaFeO_3$. In addition, Mostovoy[24] in theory proposed a phase diagram from helical AFM order to FM order by considering the charge transfer energy Δ, p–d transition integral $(pd\sigma)$, p–p transition amplitude t_{p-p}, and the superexchange coupling integral J between t_{2g} spins. In such a phase diagram, the FM order appears in the region with high $\Delta/(pd\sigma)$ value. When the lattice expands due to chemical doping, the $(pd\sigma)$ decreases rapidly. Meanwhile, the charge transfer energy does not change much. As a result, the FM order is more likely to occur with increasing lattice constant. Since the Co doping favors lattice increase, the FM ground rather than the helical AFM one emerges in the current $BaFe_{0.95}Co_{0.05}O_3$ single crystal.

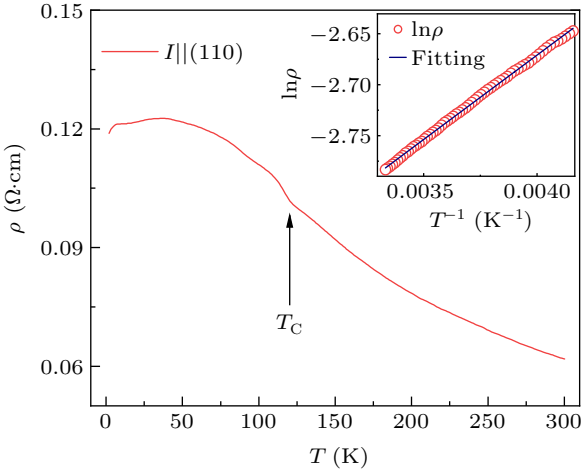

Fig. 3. Temperature dependence of resistivity for $BaFe_{0.95}Co_{0.05}O_3$ single crystal measured with electrical current parallel to the (110) plane. The inset shows the fitting result using the thermal excitation model in 240 K–300 K.

Figure 3 shows the temperature dependence of resistivity for $BaFe_{0.95}Co_{0.05}O_3$ single crystal with the current parallel to the (110) plane. The value of resistivity at 300 K is about 6.2×10^{-2} Ω·cm. As the temperature decreases, the resistivity slightly increases, suggesting a semiconducting electrical transport behavior. Once the temperature decreases to T_C, the resistivity displays a small increase. On further cooling to less than ∼ 50 K, the resistivity is nearly unchanged any more, implying a bad metal-like behavior at lower temperatures. In 240 K–300 K, the temperature dependence of resistivity can be fitted the thermal excitation model (see the inset of Fig. 3), yielding the activation energy to be 14.3 meV. Such a small activation energy as well as the bad metal-like electrical transport suggest the itinerant electronic behavior of $BaFe_{0.95}Co_{0.05}O_3$ single crystal below T_C.

To get a deeper insight into the transport properties for $BaFe_{0.95}Co_{0.05}O_3$, the temperature dependence of specific heat (C_p) was measured. As showed in Fig. 4, a λ-type anomaly is found to occur in the specific heat curve near T_C, indicating the second-order nature for the long-range FM phase transition. At the temperatures below 12 K, the specific heat data can be well fitted using the function $C_p = \gamma T + \beta T^{3/2} + \alpha T^3$ (see the inset of Fig. 4). The fitted parameters are $\gamma = 1.52(8) \times 10^{-2}$ J·mol·K^{-2}, $\beta = 2.44(3) \times 10^{-3}$ J·mol·K$^{-5/2}$, and $\alpha = 1.67(4) \times 10^{-4}$ J·mol·K^{-4}. In comparison, the value of γ coefficient is larger than that of β and α, suggesting the solid contribution of itinerant electrons in $BaFe_{0.95}Co_{0.05}O_3$. In the parent $BaFeO_3$, the fitted value of $\gamma = 2.78 \times 10^{-2}$ J·mol·K^{-2},[15] which is larger than that of the current Co-doped one. Actually, one can find an apparent metallization transition at the long-range spin ordering temperature, but the resistivity experiences a small increase in $BaFe_{0.95}Co_{0.05}O_3$. The Co introduction thus looks unfavorable for the presence of itinerant electronic behavior, probably due to the reduced p–d hybridization caused by lattice expansion.

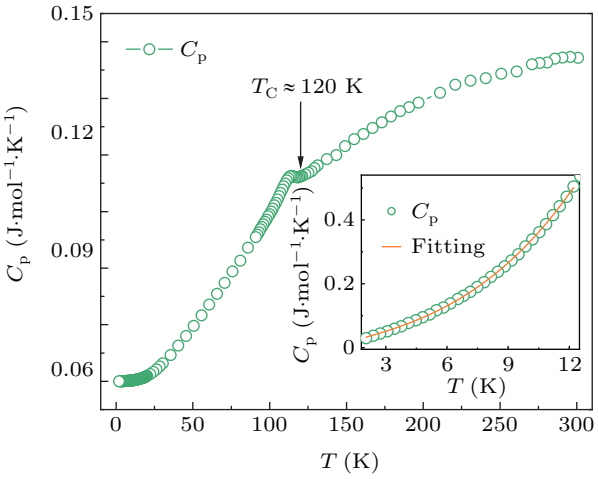

Fig. 4. Temperature dependence of specific heat for $BaFe_{0.95}Co_{0.05}O_3$ single crystal. The inset shows the fitting result for specific heat date below 12 K using the function $C_p = \gamma T + \beta T^{3/2} + \alpha T^3$.

4. Conclusion

In summary, the single crystal of $BaFe_{0.95}Co_{0.05}O_3$ was prepared by the combination of floating zone methods with high-pressure techniques for the first time. The crystal crystallizes to a simple cubic perovskite structure with Pm-3m symmetry. The TG analysis confirms the stoichiometric oxygen content for the as-made single crystal, suggesting the presence of Fe^{4+}/Co^{4+} state. Compared with parent $BaFeO_3$, the

slight introduction of Co in $BaFe_{0.95}Co_{0.05}O_3$ only induces a small lattice expansion, but essentially changes the magnetism from the initial helical AFM ground state to an FM one with the Curie temperature $T_C \approx 120$ K. The resistivity and specific heat measurements indicate that the FM ordering favors a bad metal-like electrical transport behavior in $BaFe_{0.95}Co_{0.05}O_3$. The present work shows that Co-doping is an effective method to modify the magnetic and electrical properties for the cubic perovskite of $BaFeO_3$.

Acknowledgments

Project supported by the National Natural Science Foundation of China (Grant Nos. 11934017 and 11921004), the National Key Research and Development Program of China (Grant Nos. 2021YFA1400300, 2018YFE0103200, and 2018YFA0305700), the Beijing Natural Science Foundation (Grant No. Z200007), and the Fund from the Chinese Academy of Sciences (Grant No. XDB33000000).

References

[1] Kawasaki S, Takano M, Kanno R, Takeda T and Fujimori A 1998 *J. Phys. Soc. Jpn.* **67** 1529
[2] Akao T, Azuma Y, Usuda M, Nishihata Y and Mizuki J 2003 *Phys. Rev. Lett.* **91** 156405
[3] Woodward P M, Cox D E, Moshopoulou E, Sleight A W and Morimoto S 2000 *Phys. Rev. B* **62** 844
[4] Ishiwata S, Tokunaga M, Kaneko Y, Okuyama D, Tokunaga Y, Wakimoto S, Kakurai K, Arima T, Taguchi Y and Tokura Y 2011 *Phys. Rev. B* **84** 054427
[5] Chakraverty S, Matsuda T, Wadati H, Okamoto J, Yamasaki Y, Nakao H, Murakami Y, Ishiwata S, Kawasaki M, Taguchi Y, Tokura Y and Hwang H Y 2013 *Phys. Rev. B* **88** 220405
[6] Tsuyama T, Chakraverty S, Macke S, Pontius N, Schüßler-Langeheine C, Hwang H Y, Tokura Y and Wadati H 2016 *Phys. Rev. Lett.* **116** 256402
[7] Hayashi N, Terashima T and Takano M 2001 *J. Mater. Chem.* **11** 2235
[8] Takeda T, Yamaguchi Y and Watanabe H 1972 *J. Phys. Soc. Jpn.* **33** 967
[9] Bocquet A E, Fujimori A, Mizokawa T, Namatame H, Suga S, Kimizuka N, Takeda Y and Takano M 1992 *Phys. Rev. B* **45** 1561
[10] Fujioka J, Ishiwata S, Kaneko Y, Taguchi Y and Tokura Y 2012 *Phys. Rev. B* **85** 155141
[11] Ishiwata S, Nakajima T, Kim J H, *et al.* 2020 *Phys. Rev. B* **101** 134406
[12] Shannon R D 1976 *Acta crystallographica section A* **32** 751
[13] Mori K, Kamiyama T, Kobayashi H, Otomo T, Nishiyama K, Sugiyama M, Itoh K, Fukunaga T and Ikeda S 2007 *J. App. Crystallogr.* **40** s501
[14] Hayashi N, Yamamoto T, Kageyama H, Nishi M, Watanabe Y, Kawakami T, Matsushita Y, Fujimori A and Takano M 2011 *Angew. Chem. Int. Ed.* **50** 12547
[15] Liu Y, Liu Z, Li Z, Qin S, Ye X, Shen X, Zhou B, Zhou G, Agrestini S, Valvidares M, Vasili H B, Hu Z and Long Y 2020 *Phys. Rev. B* **101** 144421
[16] Takano M, Nasu S, Abe T, Yamamoto K, Endo S, Takeda Y and Goodenough J B 1991 *Phys. Rev. Lett.* **67** 3267
[17] Kawakami T and Nasu S 2005 *J. Phys.: Condens. Matter* **17** S789
[18] Long Y W, Kaneko Y, Ishiwata S, Tokunaga Y, Matsuda T, Wadati H, Tanaka Y, Shin S, Tokura Y and Taguchi Y 2012 *Phys. Rev. B* **86** 064436
[19] Hayashi N, Yamamoto T, Kitada A, Matsuo A, Kindo K, Hester J, Kageyama H and Takano M 2013 *J. Phys. Soc. Jpn.* **82** 113702
[20] Long Y W, Kaneko Y, Ishiwata S, Taguchi Y and Tokura Y 2011 *J. Phys.: Condens. Matter* **23** 245601
[21] Larson A C and Von Dreele R B 1994 *Los Alamos National Laboratory* **86** 748
[22] Tsuyama T, Matsuda T, Chakraverty S, Okamoto J, Ikenaga E, Tanaka A, Mizokawa T, Hwang H Y, Tokura Y and Wadati H 2015 *Phys. Rev. B* **91** 115101
[23] Li Z, Laskowski R, Iitaka T and Tohyama T 2012 *Phys. Rev. B* **85** 134419
[24] Mostovoy M 2005 *Phys. Rev. Lett.* **94** 137205